International Journal on Magnetic Particle Imaging
Vol 3, No 2, Article ID 1707003, 5 Pages

Infinite Science Publishing

Research Article

Magnetic Particle Imaging of liver tumors in small animal models

Jan Dieckhoff[a,*] · Michael G. Kaul[a] · Tobias Mummert[a] · Caroline Jung[a] · Johannes Salamon[a] · Gerhard Adam[a] · Tobias Knopp[b,c] · Dorothee Schwinge[d] · Harald Ittrich[a]

[a]Department for Diagnostic and Interventional Radiology and Nuclear Medicine, University Medical Center Hamburg-Eppendorf, Hamburg, Germany
[b]Section for Biomedical Imaging, University Medical Center Hamburg-Eppendorf, Hamburg, Germany
[c]Institute for Biomedical Imaging, Hamburg University of Technology, Hamburg, Germany
[d]I. Department of Internal Medicine, University Medical Center Hamburg-Eppendorf, Hamburg, Germany
*Corresponding author, email: j.dieckhoff@uke.de

Received 22 Mai 2017; Accepted 10 July 2017; Published online 14 July 2017

Abstract

In vivo liver visualization can be realized with Magnetic Particle Imaging (MPI) since a major part of the iron oxide nanoparticles - intravenously injected and imaged with MPI - is finally taken up by the mononuclear phagocytic system (MPS) of the liver. In this study, the possibility to detect and characterize liver tumors with MPI was analyzed. Mice developing hepatocellular carcinoma (HCC) were continuously screened with high-field magnetic resonance imaging (MRI). In case of liver lesions with diameters larger 5 mm, the mice were sequentially imaged with MRI and MPI after the intravenous injection of ferucarbotran (Resovist®). For comparison of liver morphologies represented by MPI and MRI, image data of both modalities were fused assisted by external MPI and MRI fiducial markers. A good correlation between MPI and MRI images was found with image analysis-based 2-D correlation coefficients of around 0.7. Liver lesions - characterized by a missing accumulation of ferucarbotran - led to signal gaps or drops in the MPI signal depending on their actual size and location. While lesions with diameters larger than 5 mm caused visible effects in the MPI signal, smaller sized lesions did not. This was mainly attributed to the comparable low MPI resolution of a few millimeters in this study.

I. Introduction

Liver imaging is an essential tool in clinical routine since liver illnesses among tumors and metastases are of high incidence and bear an increased risk of severe disease progression [1]. Thus, excellent imaging technologies for diagnostic and interventional procedures are required. Magnetic particle imaging (MPI) - developed to monitor in vivo superparamagnetic iron oxide nanoparticle (SPION) distributions with high spatial and temporal resolution [2] - represents an interesting tool to visualize the distribution of intravenously injected SPIONs taken up by the mononuclear phagocytic system (MPS) of the liver. This concept adopts the idea of iron oxide contrast agents applied in magnetic resonance imaging (MRI) of the liver for liver lesion detection and characterization [3]. Here, an excellent contrast between liver tissue and lesion is achieved since the later, e.g., a hepatocellular carcinoma (HCC), is characterized by a missing accumulation of the iron oxide contrast agent [4]. Compared to MRI, where iron oxide loaded tissue usually causes signal loss attributed to T2 and T2* relaxation processes, the liver in MPI is directly attributed to the MPI signal because the SPIONs themselves cause the measurement signal [5]. So far, studies presenting in vivo MPI data analyzed the liver with respect to SPION body clearances [6] but not with respect to liver morphology or pathologies,

for instance, liver tumors or metastasis. To our knowledge, cancer imaging with MPI was only performed outside the liver [7].

Recently, we analyzed strategies to image the hepatic SPION distribution with MPI based on the system function approach [8]. Here, we found that for an accurate reconstruction of liver MPI data a system function is required which was measured on a sample representing the aggregation and mobility status of SPIONs taken up by liver macrophages [9]. Based on this result, we investigated in the present study the capability of MPI to visualize and characterize liver lesions in vivo. In contrast to MRI, we expected the lesions to cause signal gaps or drops in the spatial SPION distribution measured with MPI due to the commonly missing SPION accumulation in HCC.

II. Materials and Methods

II.I. Animal experiment

Genetically modified mice (Mdr2 Knockout, in-house breed, male, $n = 3$) developing inflammation induced HCC approximately one year after birth were regularly scanned with a 7 T small animal MRI system (Clinscan, Bruker BioSpin GmbH, Ettlingen, Germany). In the case of liver lesions with diameters larger 5 mm, 30 μL of ferucarbotran (Resovist®, Bayer Schering Pharma AG, Berlin, Germany) was intravenously injected into the tail vein. Ferucarbotran was developed for liver MRI and is characterized by a relatively rapid clearance from the blood stream and uptake by the MPS of the liver [10]. To avoid artifacts from SPIONs circulating in the blood stream and guarantee sufficient clearance from the blood, all mice were scanned four hours after the intravenous injection. The resulting dosage of 0.6 mmol iron per kg bodyweight (mouse weight = 25 g) is more than ten times higher than the safe dosage (40 μmol iron per kg bodyweight) applied in clinical MRI investigations. It was chosen to guarantee a high signal-to-noise ratio (SNR) for a reliable investigation of the MPI signals because the applied SPIONs do not provide an optimized MPI performance and the utilized MPI system still requires optimization with respect to the technological possible sensitivities [2]. The animal experiment was approved by the local committee on animal protection (Behörde für Gesundheit und Verbraucherschutz, Hansestadt Hamburg, No. 42/14). Animal handling, including anesthesia, body warming, positioning in the imaging systems and vital parameter monitoring, was realized according to the workflow process published by Kaul et al. [11].

II.II. MRI and MPI data acquisition

The mice were sequentially scanned in the 7 T MRI and MPI system (Philips Medical Systems DMC GmbH, Hamburg, Germany / Bruker BioSpin GmbH, Ettlingen Germany). The recorded MRI images are T1-weighted and based on a 2-D gradient echo sequence (FLASH) with 32 mm field of view (FOV), 192 × 192 matrix size, 0.8 mm slice thickness, 6 acquisitions, 48 ms repetition time and 0.77 ms echo time. The MPI data was acquired with the field free point approach scanning a 3-D volume with 2000 repetitions and a repetition time of 21.54 ms. The drive field and gradient amplitude were set to 14 mT and 1.5 T/m, respectively, resulting in a FOV of $37.4 \times 37.4 \times 18.7\,\mathrm{mm}^3$ (x-, y, z-direction). These parameters and ferucarbotran as tracer material result in a theoretical resolution in the range of $4-5$ mm corresponding to the full width at half maximum [5]. For data reconstructions according to our previous investigations [9], a system function (SF) was measured with a $2 \times 2 \times 1\,\mathrm{mm}^3$ sample containing ferucarbotran in a freeze-dried mannitol sugar matrix (c(Fe) = 100 mM). The reconstruction of the MPI data was performed with a software framework based on the programming language Julia [12] utilizing the iterative Kaczmarz method and Tikhonov regularization. Data reconstruction was performed with following parameters yielding an optimal match of MRI and MPI data: Regularization factor $\lambda = 1 \cdot 10^{-5}$, number of iterations $I = 10$, SNR threshold of 1.8 and number of averaged frames $N = 1000$.

II.III. MRI and MPI data fusion and comparison

MRI and MPI data were manually fused assisted by fiducial markers consisting of glass capillaries with an inner diameter of 1.3 mm and filled with a ferucarbotran suspension (c(Fe) = 10 mM), thus, visible in MRI and MPI [9]. MPI images were normalized to the maximum image intensity of the corresponding MPI image stack. To enable a visual comparison of both modalities in the fused images, disturbing weak MPI signals were suppressed by reducing the image intensity range of the normalized MPI images to $0.15-1$. Consequently, liver morphology and possible liver lesions can be directly compared. For a computational image analysis, the 2-D correlation coefficient r was calculated:

$$r = \frac{\sum_m \sum_n \left(R_{mn} - \bar{R}\right)\left(P_{mn} - \bar{P}\right)}{\sqrt{\left(\sum_m \sum_n \left(R_{mn} - \bar{R}\right)^2\right)\left(\sum_m \sum_n \left(P_{mn} - \bar{P}\right)^2\right)}}. \quad (1)$$

Here, R_{mn} and P_{mn} represent the pixel value with indices m and n of the equivalent MRI and MPI images. $\bar{R}$ and $\bar{P}$ express the mean pixel value of the corresponding images. Before calculating r, the measured MRI images (Fig. 1, Fig. 2, Fig. 3) were inverted and liver tissue was manually segmented on each slice resulting in MRI images presenting only liver tissue with positive contrast. Thus, r lies between 0 and 1 indicating the similarity of

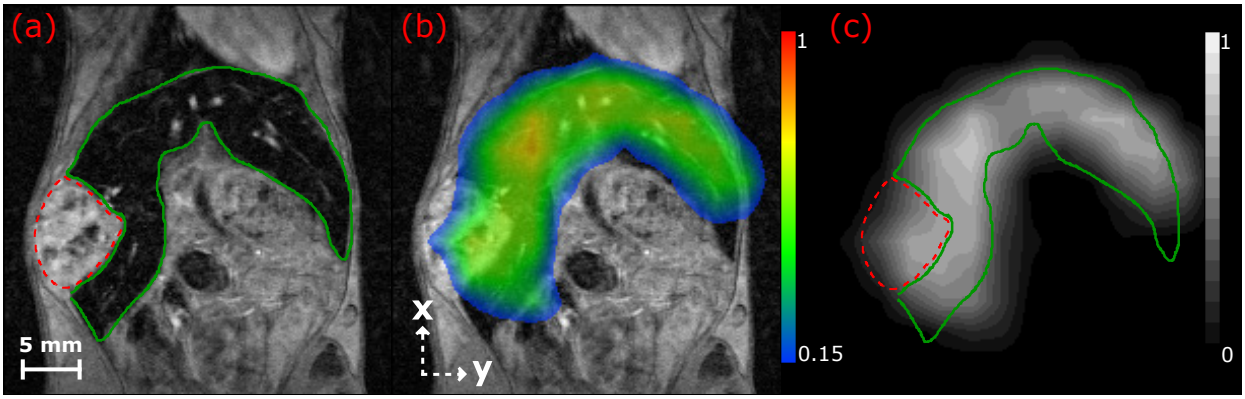

Figure 1: (a) Liver MRI (graysclae) of animal A showing contours of heterogeneous liver lesion (red dashed line) and hypointense liver tissue (green line). (b) MPI overlay (multicolor) covering the liver in the MRI image (slice 14). Dashed arrows indicate MPI scanner coordinate system. (c) Comparison of liver MPI (grayscale) and contours of liver tissue and lesion.

the compared images (maximum = 1). The coefficient r is also known as Pearson's correlation coefficient, for instance, applied for the evalutation of colocalization in microscopy techniques [13].

III. Results

The imaging results of two mice (A and B) - representing most clearly the capability of liver tumor MPI - are presented in detail in this work. A comparison of the cohort (A, B and C) is performed via the 2-D correlation coefficient.

As one can see in the MRI images, mouse A is characterized by one larger liver lesion with a heterogeneous structure and a diameter $d > 5$ mm (Fig. 1 (a)). In contrast, mouse B (Fig. 2 (a) and Fig. 3 (a)) possesses several liver lesions with hetero- and homogeneous structures. The presented heterogeneous lesions (red dashed lines) are characterized by hypointense (dark) spots within the hyperintense (bright) lesion - representing partial SPION uptake by the MPS. Fig. 1 (b), Fig. 2 (b) and Fig. 3 (b) show the fused MPI and MRI data of the corresponding slice. The MPI data was interpolated for fitting the MRI image dimensions. Here, one can see that most of the SPION loaded liver tissue of the MRI images is correctly covered by the particle distribution measured with MPI. However, partial mismatches are observable, especially in slim liver lobe corners. The indicated heterogeneous liver lesions (Fig. 1 (b)/Fig. 2 (b), red dashed lines) are mostly or completely covered by the MPI signal. On the contrary, the larger homogeneous lesion (Fig. 2 (b), yellow dotted line) is only partially covered by weak MPI signal. To illustrate these findings without the disturbing blending effect of the fused MRI and MPI data, the MPI signals are additionally displayed without MRI in Fig. 1 (c), Fig. 2 (c) and Fig. 3 (c) together with the contours determined from the corresponding MRI images. Small liver lesions (diameter < 5 mm) - especially located in the center of a liver lobe - could be detected with MRI, but did not cause any significant MPI signal drop. This can be seen in Fig. 3, where small hyperintense liver lesions (yellow dotted line) and the gall bladder (blue dashed dotted line) surrounded by hypointense liver tissue seem not to affect the measured MPI particle distribution.

The 2-D correlation coefficient calculated from the MRI and MPI data of mouse A, B and C is shown in Fig. 4 as a function of the slice number. Over a range of 15 slices (12 mm) r stays for both animals at around 0.7 indicating a constant match between MRI and MPI data for 65 % of the MPI FOV.

IV. Discussion

The comparison of the liver morphologies (contours) imaged with MRI and MPI demonstrates the principle feasibility of the liver MPI approach. A good correlation between both modalities is found, however, mismatches exist. These are mainly attributed to the comparable low resolution of MPI in connection with the specific MPI problem to resolve weak signals in the presence of much stronger ones [14]. Furthermore, motion related effects could hamper the direct comparison between MRI and MPI. For instance, animal movements of few millimeters inside the bed cannot be excluded completely during the sequential imaging procedure which requires an animal transport between the two systems (distance < 15 m). A blurring effect in the averaged MPI data resulting from respiratory motion seems to be negligible compared to the spatial resolution of MPI.

The results demonstrate that larger liver lesions (d > 5 mm) located at the liver lobe border cause an effect on the measured MPI particle distribution, especially if they are homogenously structured. For instance, the round shaped homogenous lesion in Fig. 2 is clearly re-

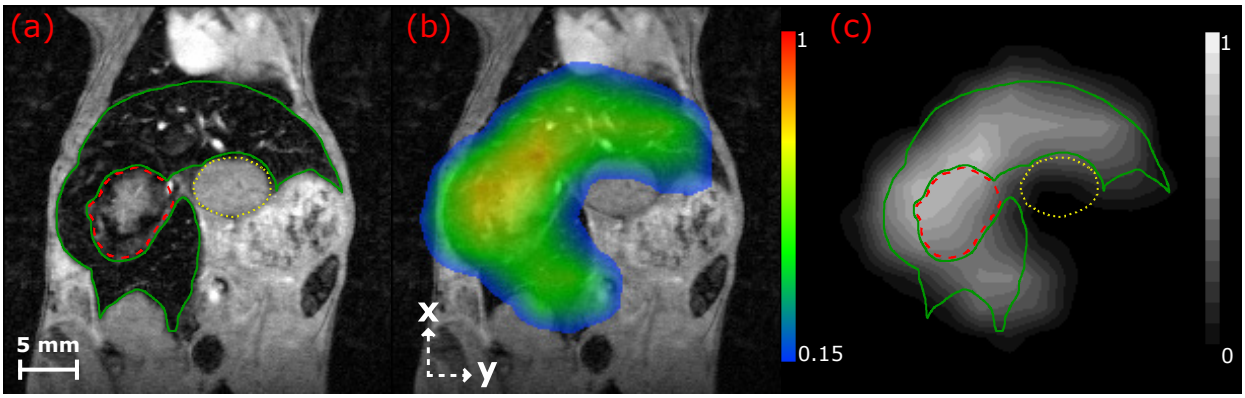

Figure 2: (a) Liver MRI (grayscale) of animal B showing contours of homogenous (yellow dotted line) and heterogeneous (red dotted line) liver lesions as well as hypointense liver tissue (green line). (b) MPI overlay (multicolor) covering the liver in the MRI image (slice 13). Dashed arrows indicate MPI scanner coordinate system. (c) Comparison of liver MPI (grayscale) and contours of liver tissue and lesions.

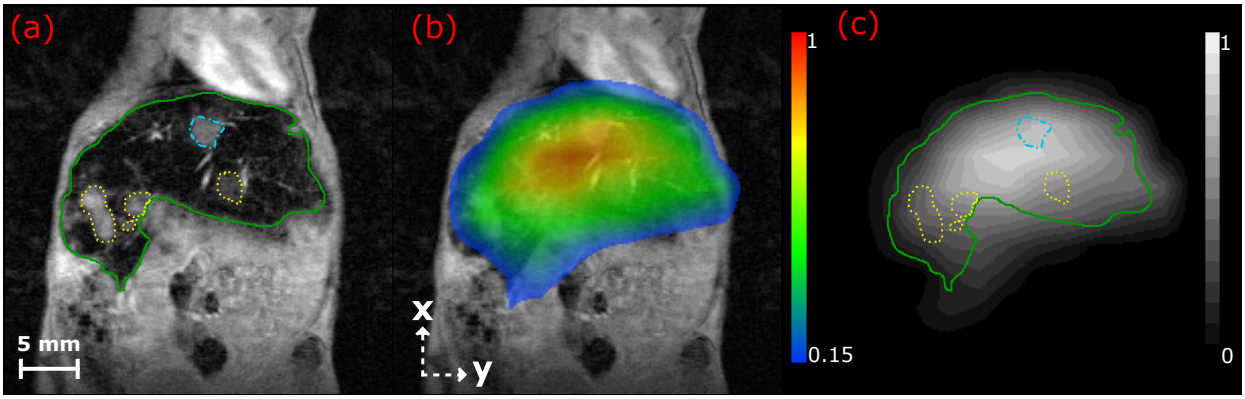

Figure 3: (a) Liver MRI (grayscale) of animal B showing contours of homogenous liver lesions (yellow dotted line) and gall bladder (blue dashed dotted line) as well as hypointense liver tissue (green line). (b) MPI overlay (multicolor) covering the liver in the MRI image (slice 10). Dashed arrows indicate MPI scanner coordinate system. (c) Comparison of liver MPI (grayscale) and contours of liver tissue, lesions and gall bladder.

flected by the border of the MPI particle distribution. In contrast, smaller liver lesions (d < 5 mm) and centrally located ones with heterogeneous structure could not be linked to gaps or drops in the MPI particle distribution (e.g. Fig. 3). The reason of this limitation is mainly attributed to the spatial resolution of the actual MPI system/protocol and the resulting partial volume effect that overlays possible lesion-induced drops in the MPI signal. The general inhomogeneity of the MPI particle distribution inside the liver contour with local maxima is a direct result of the partial volume effect and does not reflect the true distribution since ferucarbotran is not known for a significant irregular uptake by the liver MPS [10].

Volumetric analyses of liver lesions with MPI could not be performed since lesions totally surrounded by healthy liver tissue did not cause an analyzable gap in the MPI signal. The good 2-D correlation coefficient over a wide range of slices demonstrates the feasibility of MPI to perform fast real 3-D liver imaging with constant quality, which is an important issue for possible interventional liver MPI applications.

V. Conclusion

We could demonstrate the principle feasibility of liver tumor MPI by sequentially imaging tumor-bearing mice with MRI and MPI after intravenous injections of ferucarbotran, a clinically proven iron oxide contrast agent. The border between liver tissue and homogeneous liver lesions with diameters larger 5 mm could be identified in the MPI data when comparing it with the corresponding MRI data. Smaller sized and strong heterogeneous lesions did not cause consistent or visible signal drops in the MPI data. The resolution of the utilized MPI system and protocol appears to be the main limitation. Consequently, MPI-optimized SPIONs [15] need to be applied since it was shown that the spatial resolution in MPI mea-

10.18416/ijmpi.2017.1707003

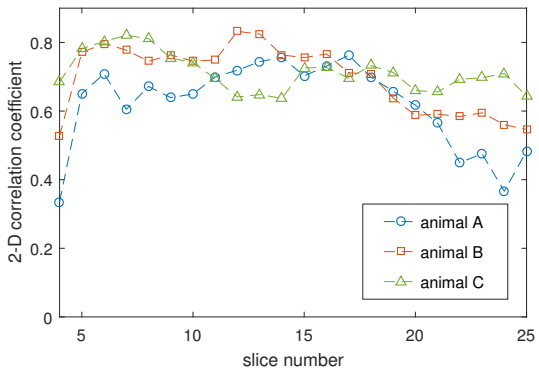

Figure 4: 2-D correlation coefficient calculated from MRI and MPI images for animal A, B and C as a function of the slice number.

surements with ferucarbotran decreases by a factor of two and more when comparing full widths at half maximum determined from magnetic particle spectroscopy measurements. Furthermore, the maximum gradient field strength of the MPI system (2.5 T/m) - not applicable during the investigations due to technical reasons - will provide higher resolution for future liver MPI investigations. In addition, the usage of improved SPIONs and an optimized MPI measurement coil will allow experiments with SPION dosages in the clinical relevant range. The analyzed liver MPI concept does not represent a competitive standalone liver tumor imaging tool compared to contrast-enhanced MRI, even not with significantly improved resolution. The missing background image will most likely hamper the diagnostic benefit. However, this static liver MPI measurement could provide important diagnostic information in combination with dynamic vascular liver MPI. Another promising application of liver MPI can be the additional imaging of SPION parameters, such as the measurement of particle temperatures to guide thermal tumor ablation therapies. With respect to instrumentation, the liver MPI concept seems very interesting for bi-modal imaging systems, e.g., a combination of MPI with MRI or computed tomography.

Acknowledgements

The authors acknowledge financial support by the Deutsche Forschungsgemeinschaft (DFG) under Sonderforschungsbereich (SFB) 841.

References

[1] S. Chacko and S. Samanta. "Hepatocellular carcinoma: A life-threatening disease". *Biomed. Pharmacother.*, 84:1679–1688, 2016. doi:10.1016/j.biopha.2016.10.078.

[2] B. Gleich and J. Weizenecker. Tomographic imaging using the nonlinear response of magnetic particles. *Nature*, 435(7046):1214–1217, 2005. doi:10.1038/nature03808.

[3] S. Saini, D. D. Stark, P. F. Hahn, J. Wittenberg, T. J. Brady, and J. T. Ferucci Jr. Ferrite particles: a superparamagnetic MR contrast agent for the reticuloendothelial system. *Radiology*, 162(1):211–216, 1987. doi:10.1148/radiology.162.1.3786765.

[4] Y. Kawamori, O. Matsui, M. Kadoya, J. Yoshikawa, H. Demachi, and T. Takashima. Differentiation of hepatocellular carcinomas from hyperplastic nodules induced in rat liver with ferrite-enhanced MR imaging. *Radiology*, 183(1):65–72, 1992. doi:10.1148/radiology.183.1.1549696.

[5] T. Knopp and T. M. Buzug. *Magnetic Particle Imaging: An Introduction to Imaging Principles and Scanner Instrumentation*. Springer, Berlin/Heidelberg, 2012. doi:10.1007/978-3-642-04199-0.

[6] B. Zheng, M. P. von See, E. Yu, B. Gunel, K. Lu, T. Vazin, D. V. Schaffer, P. W. Goodwill, and S. M. Conolly. Quantitative Magnetic Particle Imaging Monitors the Transplantation, Biodistribution, and Clearance of Stem Cells In Vivo. *Theranostics*, 6(3):291–301, 2016. doi:10.7150/thno.13728.

[7] E. Yu, M. Bishop, P. W. Goodwill, B. Zheng, M. Ferguson, K. M. Krishnan, and S. M. Conolly. First Murine in vivo Cancer Imaging with MPI. In *International Workshop on Magnetic Particle Imaging*, 2016.

[8] J. Weizenecker, B. Gleich, and J. Borgert. A simulation study on the resolution and sensitivity of magnetic particle imaging. *Phys. Med. Biol.*, 52(21):6363–6374, 2007. doi:10.1088/0031-9155/52/21/001.

[9] J. Dieckhoff, M. G. Kaul, T. Mummert, C. Jung, J. Salamon, G. Adam, T. Knopp, F. Ludwig, C. Balceris, and H. Ittrich. In vivo liver visualizations with magnetic particle imaging based on the calibration measurement approach. *Phys. Med. Biol.*, 62(9):3470–3482, 2017. doi:10.1088/1361-6560/aa562d.

[10] R. Lawaczeck, H. Bauer, T. Frenzel, M. Hasegawa, Y. Ito, K. Kito, N. Miwa, H. Tsutsui, H. Vogler, and H. J. Weinmann. Magnetic iron oxide particles coated with carboxydextran for parenteral administration and liver contrasting. Pre-clinical profile of SH U555A. *Acta Radiol.*, 38(4):584–597, 1997.

[11] M. G. Kaul, O. Weber, U. Heinen, A. Reitmeier, T. Mummert, C. Jung, N. Raabe, T. Knopp, H. Ittrich, and G. Adam. Combined Preclinical Magnetic Particle Imaging and Magnetic Resonance Imaging: Initial Results in Mice. *Fortschr. Röntgenstr.*, 187(05):347–352, 2015. doi:10.1055/s-0034-1399344.

[12] T. Knopp and M. Hofmann. Online reconstruction of 3D magnetic particle imaging data. *Phys. Med. Biol.*, 61(11):N257–N267, 2016. doi:10.1088/0031-9155/61/11/N257.

[13] K. W. Dunn, M. M. Kamocka, and J. H. McDonald. A practical guide to evaluating colocalization in biological microscopy. *Am. J. Physiol., Cell Physiol.*, 300(4):C723–C742, 2011. doi:10.1152/ajpcell.00462.2010.

[14] N. Gdaniec, M. Hofmann, and T. Knopp. Limitations of Magnetic Particle Imaging Resolving Large Contrasts. In *International Workshop of Magnetic Particle Imaging*, page 81, 2016.

[15] R. M. Ferguson, A. P. Khandhar, S. J. Kemp, H. Arami, E. U. Saritas, L. R. Croft, J. Konkle, P. W. Goodwill, A. Halkola, J. Rahmer, J. Borgert, S. M. Conolly, and K. M. Krishnan. Magnetic Particle Imaging With Tailored Iron Oxide Nanoparticle Tracers. *IEEE Trans. Med. Imag.*, 34(5):1077–1084, 2015. doi:10.1109/TMI.2014.2375065.

